

## Article

# Mesoscale Convective Systems and Extreme Precipitation on the West African Coast Linked to Ocean–Atmosphere Conditions during the Monsoon Period in the Gulf of Guinea

Sandrine Djakouré<sup>1</sup>, Joël Amouin<sup>1,2</sup> , Kouassi Yves Kouadio<sup>1,\*</sup> and Modeste Kacou<sup>1,3</sup> 

<sup>1</sup> Laboratory of Matter, Environmental and Solar Energy Sciences (LASMES), Ocean–Atmosphere Interaction Group, University Félix Houphouët-Boigny, Abidjan 22 BP 582, Côte d’Ivoire; agre.djakoure@ird.fr (S.D.); amouinjoe@asecna.org (J.A.); modeste.kacou05@ufhb.edu.ci (M.K.)

<sup>2</sup> Abidjan Meteorological Center of the Agency for the Safety of Air Navigation in Africa and Madagascar (ASECNA), Abidjan 15 BP 918, Côte d’Ivoire

<sup>3</sup> Laboratory of Matter, Environmental and Solar Energy Sciences (LASMES), Precipitation Physics Group, University Félix Houphouët-Boigny, Abidjan 22 BP 582, Côte d’Ivoire

\* Correspondence: kouassi.kouadio29@ufhb.edu.ci

**Abstract:** This study investigates the importance of convective systems for extreme rainfall along the northern coast of the Gulf of Guinea (GG) and their relationship with atmospheric and oceanic conditions. Convective system data (MCSs), daily precipitation, sea surface temperature (SST) and moisture flux anomalies from June to September 2007–2016 are used. The results show that 2/3 of MCSs crossing Abidjan are produced in June, which is the core of the major rainy season. Likewise, 2/3 of MCSs originate from continental areas, while 1/3 come from the ocean. Oceanic MCSs are mostly initiated close to the coast, which also corresponds to the Marine Heat Waves region. Continental MCSs are mostly initiated inland. The results also highlight the moisture flux contribution of three zones which have an impact on the onset and the sustaining of MCSs: (i) the seasonal migration of the intertropical convergence zone (ITCZ), (ii) the GG across the northern coastline, and finally (iii) the continent. These contributions of moisture fluxes coincide with oceanic warming off Northeast Brazil and the northern coast of the GG both two days before and the day of extreme rainfall events. The ocean contributes to moisten the atmosphere, and therefore to supply and sustain the MCSs during their lifecycle.

**Keywords:** mesoscale convective system; extreme rainfall; West African Monsoon; ocean–atmosphere conditions; Gulf of Guinea



**Citation:** Djakouré, S.; Amouin, J.; Kouadio, K.Y.; Kacou, M. Mesoscale Convective Systems and Extreme Precipitation on the West African Coast Linked to Ocean–Atmosphere Conditions during the Monsoon Period in the Gulf of Guinea. *Atmosphere* **2024**, *15*, 194. <https://doi.org/10.3390/atmos15020194>

Academic Editors: Wei Zhang, Duo Chan, Jie Feng and Yulong Yao

Received: 28 August 2023  
Revised: 29 September 2023  
Accepted: 11 October 2023  
Published: 2 February 2024



**Copyright:** © 2024 by the authors. Licensee MDPI, Basel, Switzerland. This article is an open access article distributed under the terms and conditions of the Creative Commons Attribution (CC BY) license (<https://creativecommons.org/licenses/by/4.0/>).

## 1. Introduction

West Africa belongs to the intertropical zone where the most intense convective systems occur at local, synoptic, and mesoscale scales [1]. These systems are responsible for more than 80% of cloud cover and contribute to 90% of the cumulative rainfall of this region [2]. In recent decades, this region has repeatedly experienced the severe impacts of convective systems, leading to devastating consequences for local communities. These impacts result, sometimes, in extreme rainfall events that cause loss of human life and property, road and social infrastructure damage, destruction of habitats, and disruption of water and energy resources [3,4]. Rainfall from these systems is a key parameter that determines climatic variability and helps to differentiate climatic zones in West Africa [5,6]. This last region includes some of the world’s poorest countries. Thus, its strong dependency on agricultural resources leads to disastrous consequences if abnormal situations of intense rainfall or drought occur [7].

Côte d’Ivoire is a West African country located on the edge of the tropical Atlantic Ocean, between 9° W–2.5° W of longitude and 4° N–11° N of latitude. It also experiences

climatic fluctuations marked by severe droughts, such as those of 1983 and 1994, which had a significant economic and social impact [8,9]. These resulted in an increase in bush fires, the loss of some cash crops, and lower yields of food crops [10]. This country also experienced exceptional rainfall in 2015 [3], 2014, 2017, and 2018 [11], which also had negative socio-economic impacts. It is influenced by humid air masses (hereinafter monsoon) from May to September, by the seasonal migration of the Intertropical Convergence Zone (ITCZ), and by dry air masses (hereinafter harmattan) from December to March. The District of Abidjan (centred on 5.3° N; 4.013° W) is the economic capital of Côte d'Ivoire. It is the largest metropolis that concentrates the main economic and industrial activities. It covers 2119 km<sup>2</sup>, with 14 municipalities, and has a population of 6,321,017 inhabitants, according to the latest census carried out by the Institut National de la Statistique (INS) in 2021 (<http://www.ins.ci/>, accessed on 17 August 2022). According to the report from the Office for the Coordination of Humanitarian Affairs [12], 26% of the surface area of Abidjan is at risk of flooding or landslides. Flooding and landslides caused by intense and extreme rainfall are the main natural hazards in this city, leading to loss of life and habitat, especially for vulnerable social groups [13]. For example, the Direction de la Météorologie Nationale (DMN) recorded a heavy rainfall amount of 105 mm on 11 June 2019. This event caused flooding and landslides in the communes of Yopougon, Attécoubé, Cocody and Abobo. It also caused the destruction of housing, submerged roads, and loss of human life and property, with 22 people dead, 6 people missing, 7 people injured, as well as 48 families and 121 students left homeless. However, UN-HABITAT [13] also questioned the uncontrolled occupation of roads and the lack of updating of the urbanization plan, which leads to bad expansion of the city.

The disastrous consequences of these exceptional rainfall events associated with mesoscale convective systems (hereafter MCSs) require a better understanding of the interannual variability of both parameters and of the atmospheric and oceanic surface conditions that cause these events. Many studies have suggested a relationship between the Atlantic Ocean and rainfall in West Africa [4,6,14,15], and an influence of the combination of atmospheric and oceanic surface conditions on rainfall in West Africa [3,11]. These studies have shown that sea surface temperature (SST) anomalies provide favourable conditions for the intrusion of the monsoon flow over West Africa. Most of the studies linking these dramatic rainfall events to ocean conditions generally focus on all of West Africa [16] or on the Sahel [4,17]. Few studies have been carried out along the coast of the Gulf of Guinea [6,11,18]. Similarly, various studies on convective systems in the intertropical zone [1,19–21] have mainly focused on the Sahelian region of West Africa [2,22,23]. Only few studies relate MCSs to extreme rainfall in the south of West Africa [24,25]. Finally, little is known about the MCS–extreme rainfall–atmosphere–ocean surface conditions relationships along the coast of the Gulf of Guinea.

Therefore, this study aims to establish a relationship between the convective systems that cross the coast of the Gulf of Guinea—mainly the Abidjan district—extreme rainfall events that occur there, and the atmospheric and oceanic surface conditions that cause these events. The objective is to provide a better understanding of the dynamics of convective systems on the West African coast and their contribution to the occurrence of extreme rainfall events that have dramatic economic and social impacts. Such a study is important to help decision-makers to find suitable adaptation and mitigation solutions to the risks associated with dramatic events, particularly for civil defence and urban planning.

## 2. Data and Methods

### 2.1. Data

The District of Abidjan (5.3° N; 4.013° W) covers an area of 2119 km<sup>2</sup>. It is one of the economic hubs of West Africa. Its harbour is the biggest in West Africa and the second biggest in Africa after that of Durban in South Africa. This region has a bimodal seasonal cycle centered on June and October, which represent the peaks of the major and minor rainy seasons, respectively (Figure 1). These two rainy seasons are separated by a major

dry season from December to February and a minor dry season from July to September. Annual rainfall amounts range between 1500 mm and 2000 mm.

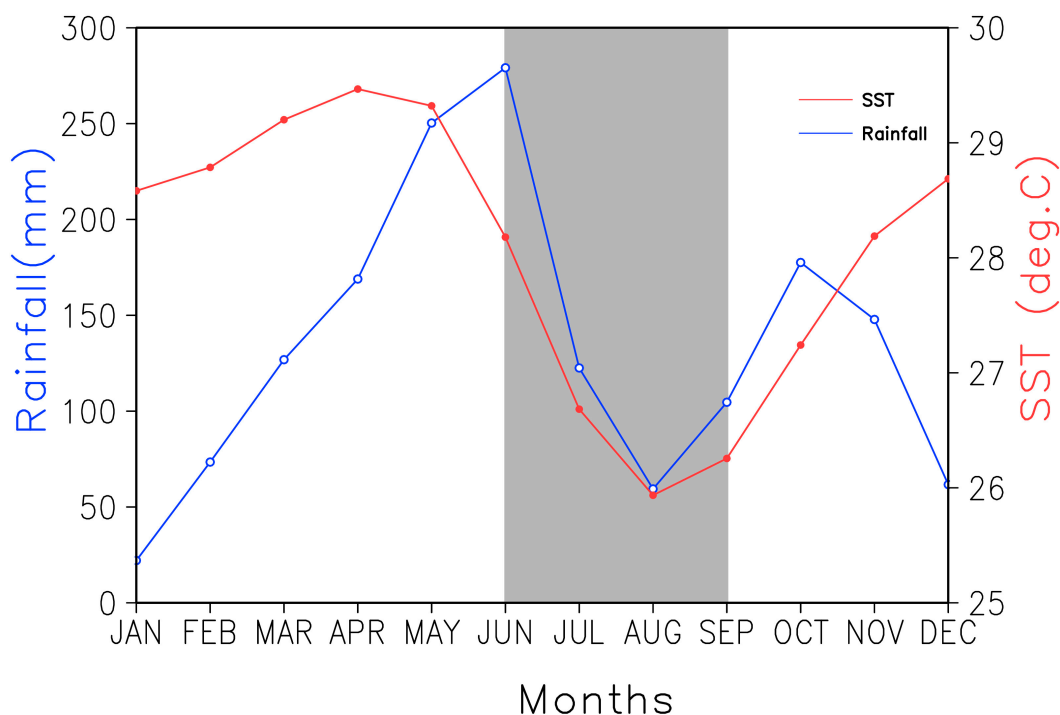


**Figure 1.** Seasonal cycle of GPCP rainfall in Abidjan and SST at the northern coast of the Gulf of Guinea over 2007–2016, averaged over  $10^{\circ}$  W– $10^{\circ}$  E;  $2^{\circ}$  N– $5^{\circ}$  N. The grey rectangle indicates the study period.

Abidjan borders the tropical Atlantic Ocean through the Gulf of Guinea. The marine seasons off the Abidjan district have been well described by various authors. The major upwelling season from July to September coincides with the monsoon period over West Africa, when the ITCZ migrates northwards [26]. Extreme rainfall over Abidjan is analyzed in relation to convective systems and surface atmospheric and oceanic conditions during the monsoon period. The rainfall variability was therefore studied by using daily values from the Global Precipitation Climatology Project (GPCP) [27] for June to September. This monsoon period includes both the peak in June of the major rainy season in Abidjan, and the upwelling period from July to September, which corresponds to the minor dry season in Abidjan. Amouin et al. [11] noted that extreme rainfall that causes disastrous social and economic consequences in the Abidjan district are found mainly in June. The daily GPCP rainfall was extracted on a  $1^{\circ} \times 1^{\circ}$  regular grid in this period from 2007 to 2016 (i.e., a total of 1220 days). This dataset was deduced from the blending of in situ observations and microwave measurements carried out by various geostationary satellites.

MCSs are usually identified by satellite digital images in the thermal infrared channel [23] and by meteorological radar [28]. In this work, the outputs of the tracking of organized convection algorithm (TOOCAN), developed by Fiolleau and Roca [23], over West Africa were used. These data are available for JJAS from 2007 to 2016. Mathon et al. [2] noted that Meteosat images are useful for cloud system characterization and classification predominantly in West and Central Africa, where the convection is well defined on a very large scale. TOOCAN uses data from the  $10.8 \mu\text{m}$  channel of METEOSAT Second Generation to provide a coherent description of the lifecycle of convective systems (initiation, maturity, and dissipation). These data have a 3 km spatial resolution and a 15 min temporal resolution. They cover West Africa and a part of the Gulf of Guinea, within the band  $0^{\circ}$  N– $19^{\circ}$  N;  $42^{\circ}$  E– $18^{\circ}$  W, over the period June–September (hereafter JJAS) from 2007 to

2016. For more details about this algorithm, the reader should refer to the paper published by Fiolleau and Roca [23].

The relationship between MCS, extreme rainfall and large-scale atmospheric and ocean surface conditions was established by using the sea surface temperature (SST), horizontal and vertical winds, and specific humidity. The sea surface conditions were documented for the tropical Atlantic using the National Oceanic and Atmospheric Administration (NOAA) Optimum Interpolation (OI) daily sea surface temperature anomalies [29]. These data were reported on a  $0.25^\circ \times 0.25^\circ$  grid for 2007–2016. Horizontal and vertical wind fields and specific humidity were extracted from the National Center for Environmental Prediction–National Center for Atmospheric Research (NCEP–NCAR) reanalysis dataset [30] for the same periods (2007–2016). Daily data were reported on a  $2.5^\circ \times 2.5^\circ$  grid, with 17 pressure levels from 1000 hPa to 10 hPa for horizontal and vertical wind and 8 pressure levels from 1000 hPa to 10 hPa for specific humidity, respectively.

## 2.2. Methods

Statistical methods were used to study MCSs and extreme rainfall variability, and to establish the relationships between these two last parameters and atmospheric and oceanic surface conditions. An intense precipitation event is defined as the exceedance of a threshold that corresponds to the daily rainfall amount exceeding a given value during the study period [31]. Here, the extreme value was defined by using percentiles that are statistical quantities [3,11,32–35]. However, there is no fixed value chosen for all months. The high variability of rainfall (~279 mm in June, ~59 mm in August, and finally ~100 mm in September according to GPCP rainfall estimates, see Figure 1) makes it difficult to set a common percentile value. Thus, the 95th percentile was chosen as the threshold for determining extreme daily values. It was computed for each month of the JJAS season (Table 1). For example, the threshold for June (24.45 mm) was calculated using a 300-day number between 2007 and 2016. This simple method makes it possible to take into account the particularities of each month in the study period. For instance, June had a greater threshold than August, which is consistent with seasonal variability.

**Table 1.** The 95th percentile threshold value of daily rainfall for each month.

Months	June	July	August	September
Threshold (mm)	24.45	17.19	8.35	12.17

During their lifespan, MCSs can move, change, grow, shrink, split, or merge into one or more systems. Here, the aim was to determine their trajectory, from initiation to dissipation. At the date of extreme rainfall over Abidjan, MCSs that partially or entirely cover the city were identified. From this date, the trajectory of the convective system was investigated to establish the zones of initiation and dissipation. In this study, no assumptions were made about the convective zone of the MCS which would produce rain, nor about the part of Abidjan which would receive the rain. The entire MCS selection method is described in Appendix A.

The study of the specific atmospheric circulation and ocean surface conditions that can help to understand the role of MCSs in the occurrence of extreme rainfall events was achieved by plotting composite patterns of SST and horizontal moisture flux anomalies at 850 hPa, 925 hPa, and 1000 hPa each month. Moisture flux anomalies were calculated from the product of the wind and specific humidity anomalies. Discriminating atmospheric levels allows the analysis of the atmospheric dynamics that could influence these events. Anomalies were calculated as the difference between the same calendar days of the variable and its long-term daily mean. Then, the composite patterns were obtained by averaging each variable over all days of extreme events associated with the MCSs. Significant values derived from the *t*-test were also plotted. This method is fully described in Brown et al. [36].

### 3. Results and Discussion

#### 3.1. MCS Occurrence along the Coast during JJAS

MCSs crossing the Abidjan district were identified in the dataset. At the time when a part or the entire surface of the convective system was over the Abidjan district, the trajectories were tracked. They included all positions from initiation to dissipation. The reader can refer to the Appendix A for further explanation of this method. A MCS is oceanic (resp. continental) if its center of mass at initiation is located in the ocean (resp. continent).

The number and monthly frequencies of MCSs were computed during the monsoon period (Table 2 and Figure 2). A total of 582 convective systems were identified, of which 386 (~66.32%) were continental MCSs and 196 (~33.68%) were oceanic MCSs (Table 2). Table 2 shows that 2/3 (~64.78%) of the MCSs that crossed Abidjan occurred in June, which is the core of the rainy season. This number dropped significantly in July (19.24%) and in August (4.30%), which is the period of coastal upwelling at north of the Gulf of Guinea. The lower value in August coincides with the intensification of ocean cooling. The cooling of the coastal waters could help to stabilize the oceanic air masses and to prevent MCS initiation. Similarly, this period corresponds to the northernmost position of ITCZ [37,38], which influences the rainfall in the north of Côte d’Ivoire [5] and in the Sahel [4]. The slight increase in MCSs (~11.66%) in September is related to the end of the upwelling season and the beginning of the short rainy season along the coast. This is consistent with the seasonal cycle (see Figure 1), in which rainfall rises after the drop in August.

**Table 2.** Number of MCSs per month recorded in the Abidjan district in JJAS. The values in brackets represent the percentage of these systems relative to the total number.

Months	Total MCS	Continental MCS	Oceanic MCS
June	377 (64.77%)	225 (38.66%)	152 (26.12%)
July	112 (19.24%)	77 (13.23%)	35 (6.01%)
August	25 (4.30%)	20 (3.44%)	5 (0.90%)
September	68 (11.66%)	64 (11.00%)	4 (0.69%)
Total	582 (100%)	386 (66.32%)	196 (33.68%)

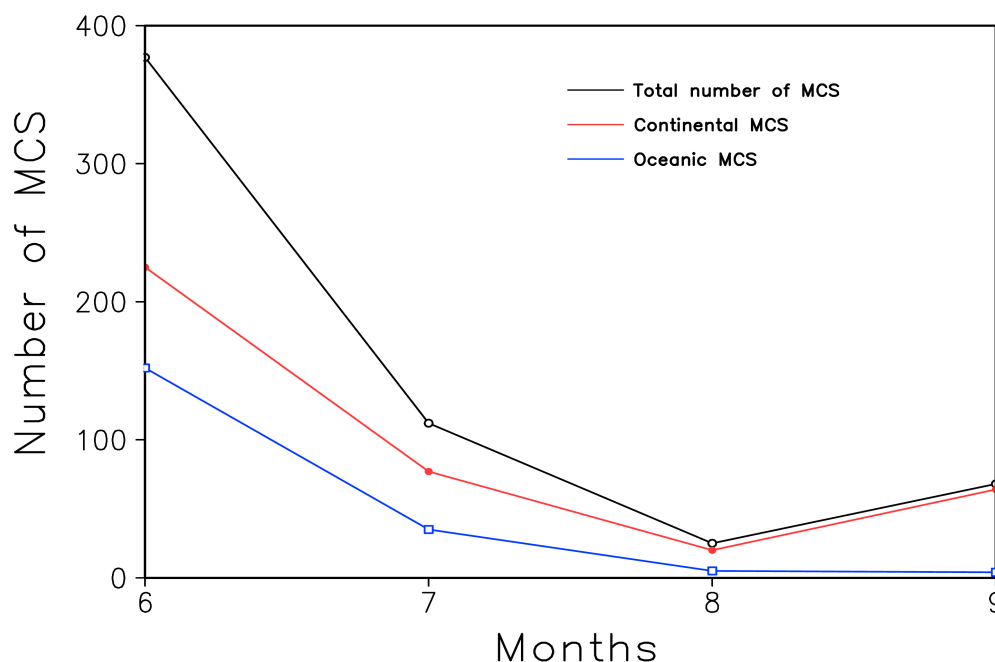


**Figure 2.** Monthly evolution of MCS numbers (black) recorded in the Abidjan district during JJAS from 2007 to 2016. Continental (red) and oceanic (blue) MCSs are also represented.

Discrimination between convective systems showed that 2/3 (~66.52%) were continental, while 1/3 (~33.68%) were oceanic. The evolution of continental MCSs was similar to the total number during the monsoon period. It moved from the highest value in June (~38.66%) to the lowest in August (~3.44%), followed by a relative increase in September (~11.0%). The number of oceanic MCSs decreased from June (~26.12%) to September (~0.69%). This would indicate that the ocean's contribution to coastal rainfall, through the convective systems, declines and disappears as the monsoon season nears its end.

Figure 3 shows the spatial distribution of the centers of mass of the MCSs during both initiation (Figure 3a) and dissipation (Figure 3b). The initiation and dissipation coordinates of these systems are represented by red dots for continental systems and green dots for oceanic systems. In order to take into account the entire lifespan of the system, the initiation (resp. dissipation) coordinates match the MCS positions in the first (resp. last) satellite image, where the brightness temperature is below (resp. above) the 235 K threshold. MCS surfaces at each timestep were not considered. This figure shows that the MCSs moved predominantly westwards and were either oceanic or continental.

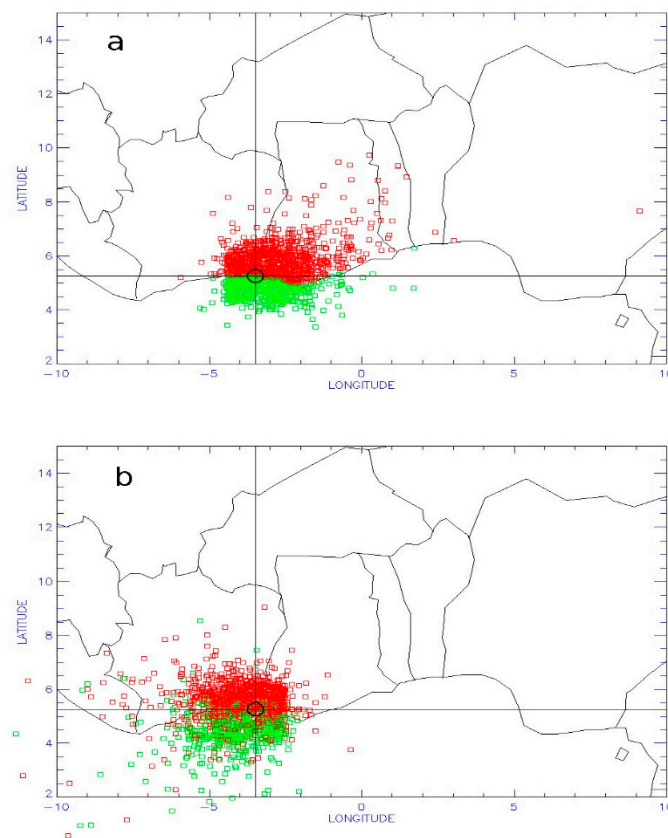


**Figure 3.** (a) Initiation and (b) dissipation coordinates of oceanic (green) and continental (red) MCSs crossing Abidjan during JJAS from 2007 to 2016. Longitude (vertical black line) and latitude (horizontal black line) cross at the Abidjan district (black circle).

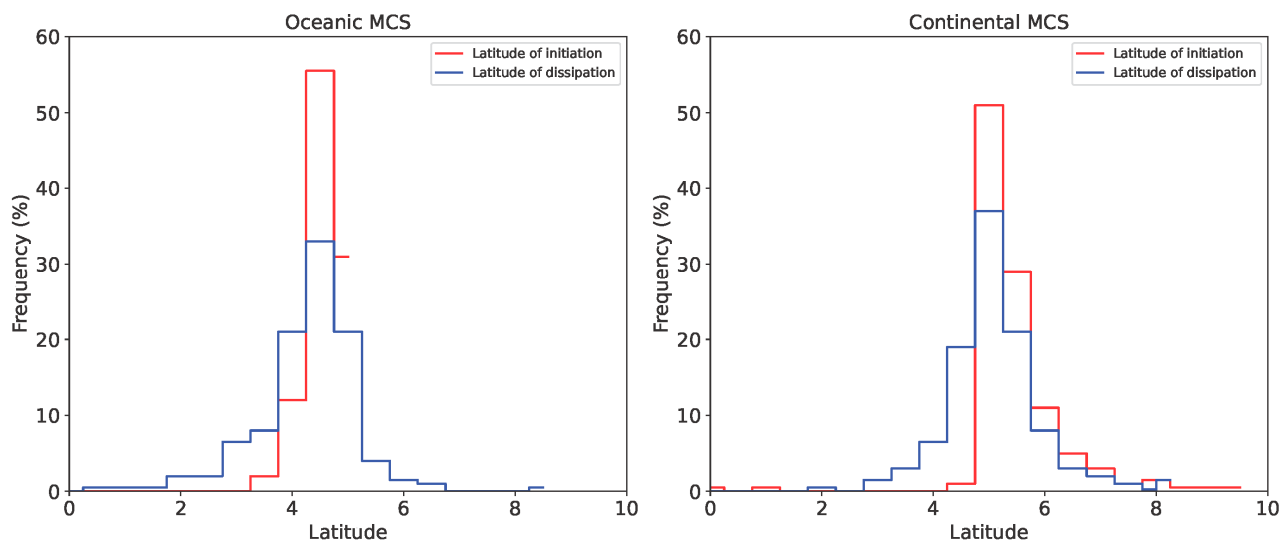
Oceanic MCSs (Figure 3a) were mainly initiated between  $5^{\circ}\text{W}$ – $1^{\circ}\text{E}$ ;  $3.5^{\circ}\text{N}$ – $5^{\circ}\text{N}$ , near the coast. This band is known as the coastal upwelling region in the north of the Gulf of Guinea [39]. It also corresponds to the region of marine heatwaves [40] which influence the climate of the coastal countries of West Africa. The dissipation of these MCSs occurred essentially in four regions: (i) The first region relates to the  $5^{\circ}\text{W}$ – $1^{\circ}\text{E}$ ;  $3.5^{\circ}\text{N}$ – $5^{\circ}\text{N}$  band where they are initiated. (ii) The second region lies south of  $3.5^{\circ}\text{N}$ , from  $1^{\circ}\text{N}$  to  $3.5^{\circ}\text{N}$ . These two areas were the most frequent regions of dissipation. (iii) The third region lies westward between  $12^{\circ}\text{W}$  and  $8^{\circ}\text{W}$ . (iv) Finally, the last region lies to the north, between  $5^{\circ}\text{N}$  and  $9^{\circ}\text{N}$ . These last two areas recorded the lowest numbers of MCS dissipation.

Most of the continental MCSs (Figure 3b) were initiated in Côte d'Ivoire and Ghana, between the coastline at  $5.15^{\circ}$  N and  $6^{\circ}$  N. The second area of frequent initiation was the middle of Côte d'Ivoire ( $6^{\circ}$  N to  $9^{\circ}$  N) and the east of Ghana, where few MCSs were initiated. Finally, a zone between  $6^{\circ}$  E and  $10^{\circ}$  E recorded a MCS with both the longest trajectory and lifecycle. This last zone corresponds closely to the Joss plate in Nigeria, which is a frequent zone of MCS initiation [3].

### 3.2. Spreading and Daily Convective Activity of MCSs along the Coast

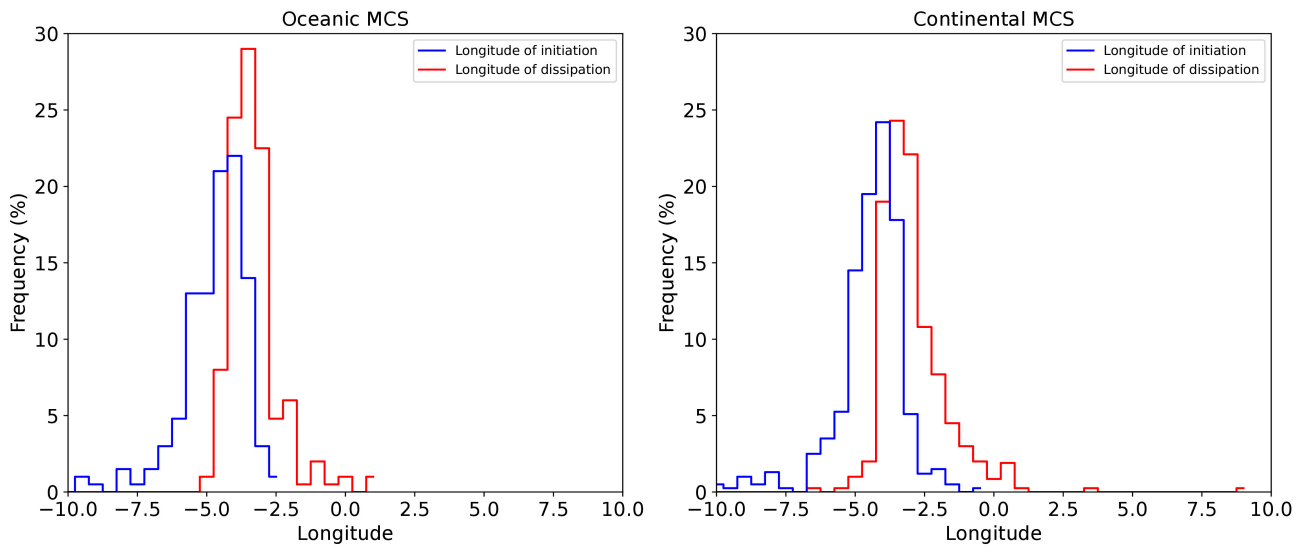
The MCS initiation or dissipation coordinates were classified in  $0.25^{\circ}$  equal-amplitude classes, between  $0^{\circ}$  N and  $10^{\circ}$  N of latitude and  $10^{\circ}$  W and  $10^{\circ}$  E of longitude, respectively, to study both latitudinal and longitudinal displacements. For daily convective activity, 0.5 h equal-amplitude classes were defined from 0 to 24 h. Then, the frequencies of initiation and dissipation coordinates and the daily convective activity were calculated.

Figure 4 illustrates the latitudinal evolution of continental and oceanic MCSs. The maximum frequencies of initiation and dissipation of oceanic MCSs reached  $\sim 53\%$  and  $\sim 33\%$  respectively at around  $4.5^{\circ}$  N (Figure 4, left). The spreading of the initiation curve between  $3.5^{\circ}$  N and  $4^{\circ}$  N indicates that these systems were mostly initiated off the coast. Most of these systems dissipated over the ocean between  $2^{\circ}$  N and  $4.5^{\circ}$  N, and some of them over the coast between  $4.5^{\circ}$  N and  $6.5^{\circ}$  N. The maximum frequencies of initiation and dissipation of continental MCSs reached  $\sim 50\%$  and  $\sim 36\%$ , respectively, at around  $5^{\circ}$  N (Figure 4, right). Most MCSs were initiated along the coast from  $4.5^{\circ}$  N to  $7^{\circ}$  N, and few between  $7^{\circ}$  N and  $9^{\circ}$  N. The dissipation of these systems was almost evenly distributed across the  $2^{\circ}$  N– $8^{\circ}$  N band, centered at  $5^{\circ}$  N, where the maximum frequency was noted.



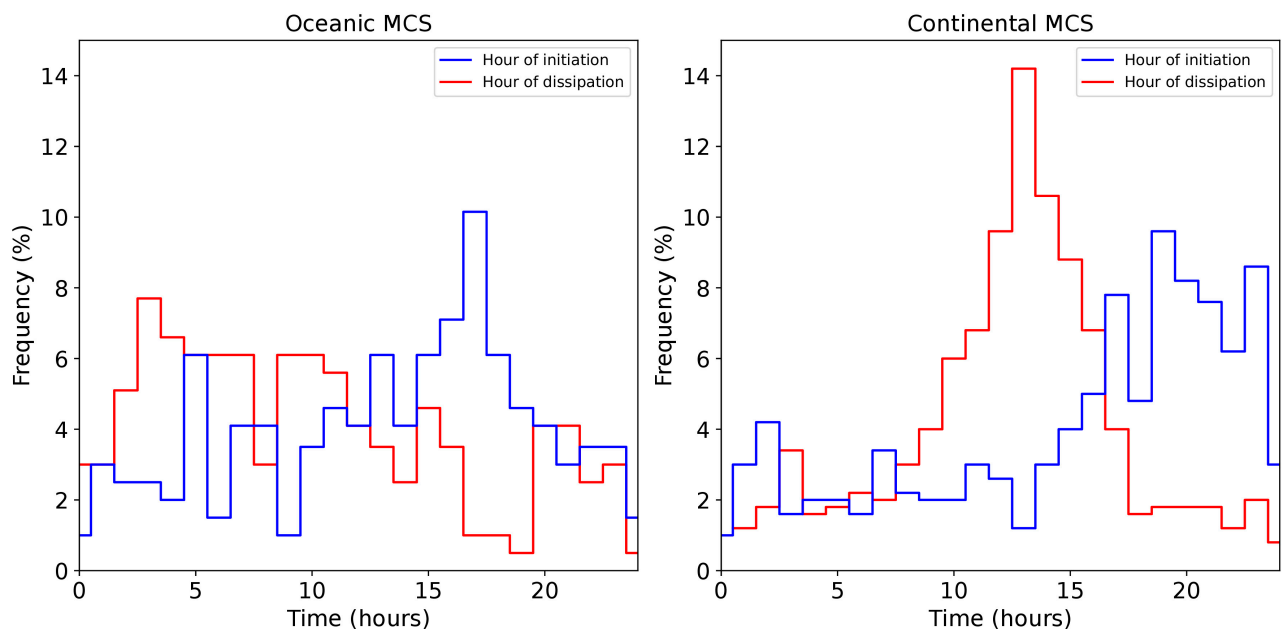
**Figure 4.** Latitudinal displacement of oceanic (left) and continental (right) MCSs crossing the Abidjan district during JJAS from 2007 to 2016.

Figure 5 shows the longitudinal evolution of MCSs. The maximum frequencies of initiation and dissipation of oceanic MCSs reached 29% at around  $3.5^{\circ}$  W and 22% at  $4^{\circ}$  W, respectively (Figure 5, left). The initiation curve extends eastwards between  $5^{\circ}$  W and  $0^{\circ}$  E. This longitudinal band corresponds to the coastal upwelling zone in the north of the Gulf of Guinea [40]. Most of these MCSs dissipated westwards between  $10^{\circ}$  W and  $2.5^{\circ}$  W, outside the coastal upwelling zone. The maximum frequencies of initiation and dissipation of continental MCSs reached  $\sim 25\%$  at around  $3.5^{\circ}$  W and  $4^{\circ}$  W, respectively (Figure 5, right), and were initiated at between  $5^{\circ}$  W and  $2.5^{\circ}$  W, respectively. The spreading of the dissipation curve at around  $10^{\circ}$  W indicates a westward propagation of these convective systems.



**Figure 5.** Same as Figure 4, but for the longitudinal displacement of the MCSs.

Figure 6 shows the daily convective activity of the MCSs. The minimum and maximum durations of their lifecycles were 02h and 39.5h, respectively (not shown). Most of the oceanic MCSs were initiated between 00h UT and 10h UT and dissipated between 14h UT and 20h UT (Figure 6, left). In the case of continental MCSs, initiation occurred between 10h UT and 16h UT, while dissipation took place between 16h UT and 00h UT (Figure 6, right). These results are in agreement with Rasera et al. [41], who pointed out a difference between MCS initiation and dissipation on the continent and in the ocean. Indeed, the initiation period of continental systems coincides with the maximum convection on the continent, which supplies these MCSs with moisture fluxes during their lifecycle.



**Figure 6.** Daily convective activity of oceanic (left) and continental (right) MCSs crossing the Abidjan district during JJAS from 2007 to 2016.

### 3.3. Relationship between MCSs and Extreme Rainfall along the Coast of the Gulf of Guinea

The aim of this section is to understand the influence of MCSs in the occurrence of extreme rainfall events in the Abidjan district. Figure 7 shows the interannual evolution of cumulative rainfall during JJAS of each year. It also displays the cumulative rainfall of

extreme rainfall events and the number of MCSs recorded in the Abidjan district for the same period. From 2007 to 2016, the highest cumulative rainfall amount in JJAS occurred in 2010 and 2014, while the lowest cumulative rainfall amount was in 2012. The trend in this interannual evolution decreased, although this was not significant (not shown). The trend of the cumulative extreme rainfall was similar to that of the total rainfall amount. Extreme rainfall accounted for ~35% of the total cumulative rainfall on average. It reached almost ~48% in 2010 and 2014, which were the wettest years in the series. The number of extreme rainfall events that allowed this contribution was 11 and 10 in 2010 and 2014, respectively (not shown). The low number of extreme rainfall events indicates that most of the cumulative annual rainfall during JJAS is due to a few rainfall events which can have disastrous consequences for the region. MCSs followed a similar interannual evolution to that of cumulative extreme and cumulative total rainfall amounts. A higher (lower) MCS number was associated with a heavily (weakly) rainy year. This result would indicate a relationship between MCS occurrence and extreme rainfall in the Abidjan district.

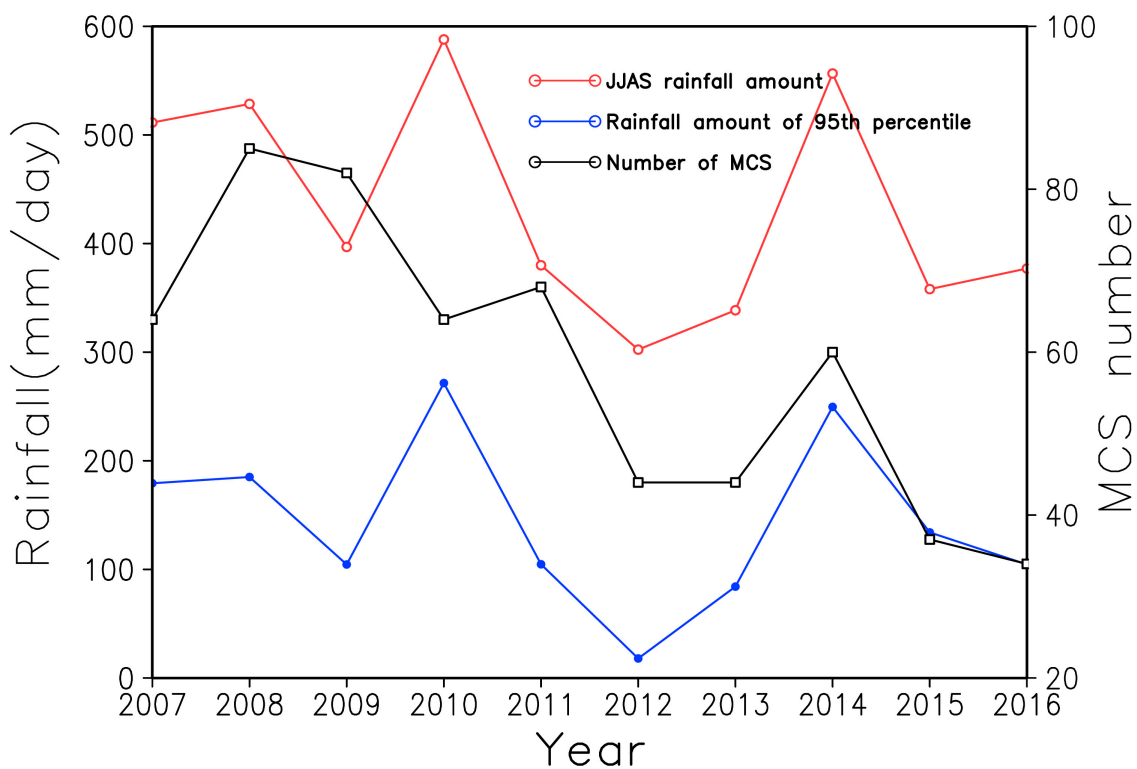


**Figure 7.** Interannual evolution of total cumulative rainfall, extreme rainfall, and MCS number recorded over the Abidjan district during JJAS from 2007 to 2016.

Figures 8 and 9 illustrate the combined daily variation of rainfall and the number of MCSs recorded in the Abidjan district for each year in JJAS. The selected events are marked by black bars for one or more successive days. Extreme rainfall events for which the threshold is above the 95th percentile are shown in grey. MCSs have been differentiated into continental and oceanic.

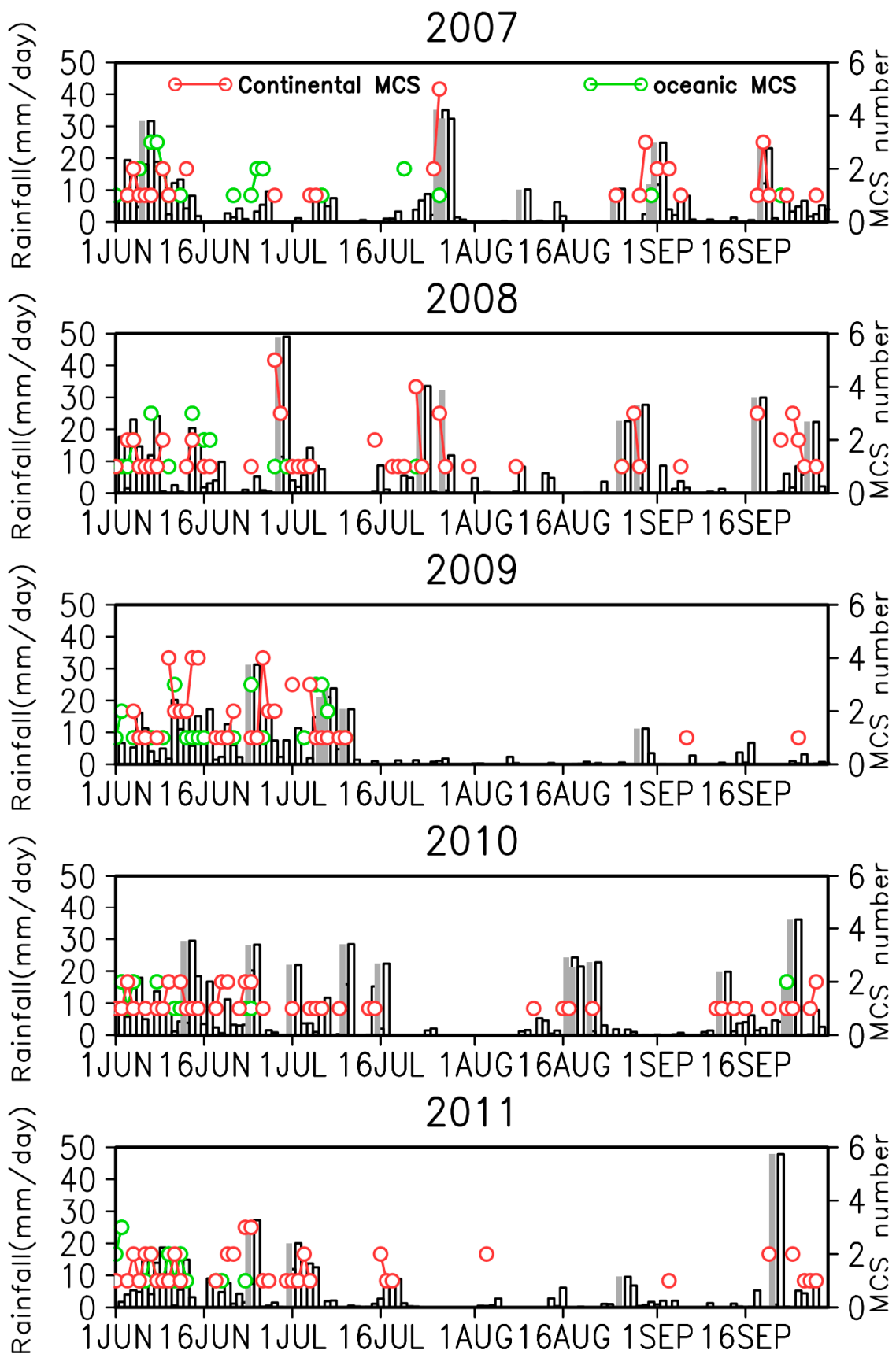


**Figure 8.** Daily rainfall (bars) and MCS number (circles) recorded in the Abidjan district from 2007 to 2011. The grey bars represent extreme rainfall values above the 95th percentile threshold.

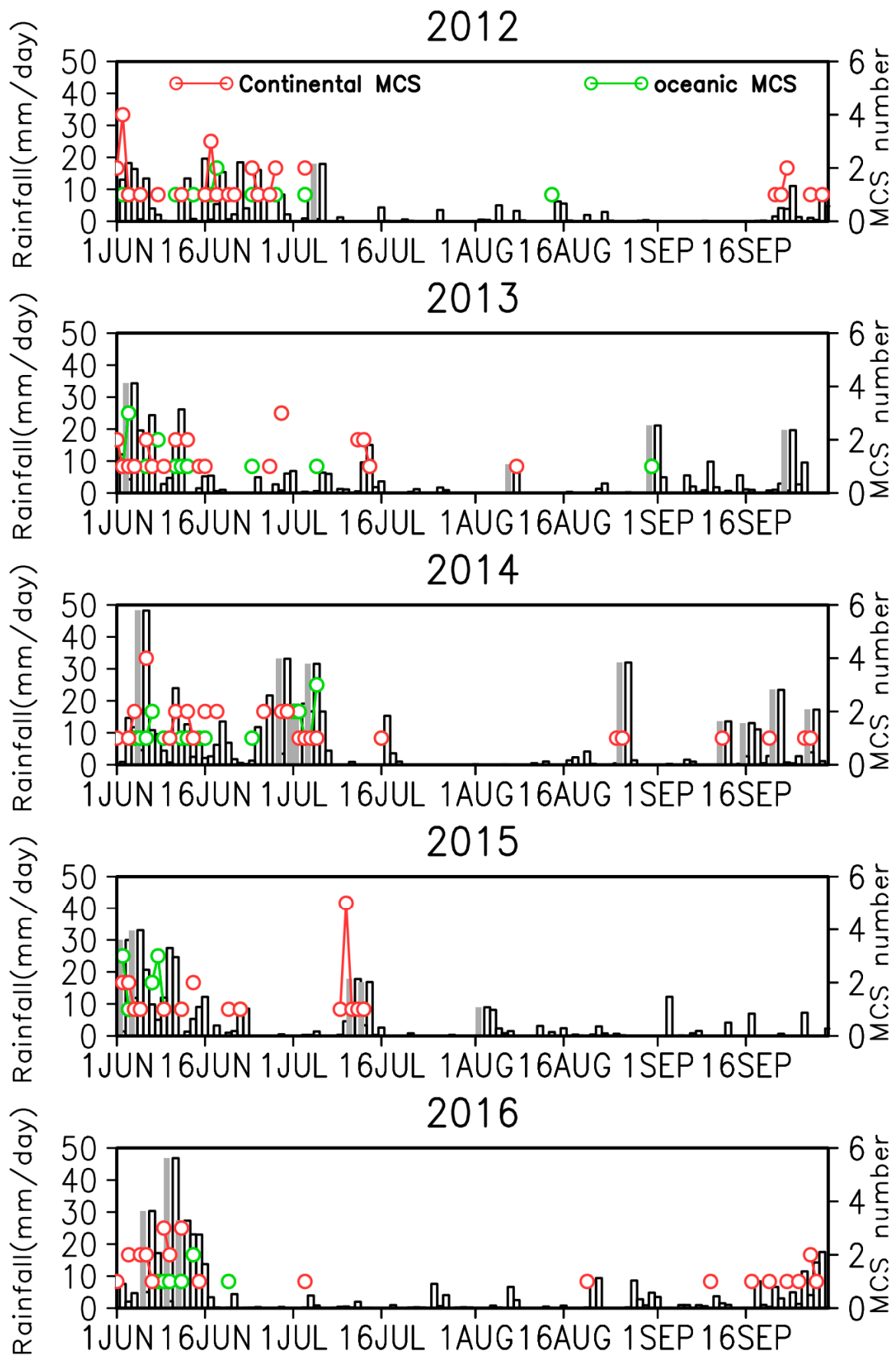


Figure 9. Same as Figure 8, but for 2012 to 2016.

Extreme rainfall occurred mainly in June and the first half of July, and in September, when rainfall rose again in accordance with the seasonal cycle. In particular, September recorded numerous extreme events in 2008 and 2010 (Figure 8), and 2014 (Figure 9).

The frequency of MCS occurrence was similar to that of extreme rainfall events. Each extreme event seems to be associated either with the occurrence of oceanic or continental convective systems, or both. This combination of extreme events and the concomitant occurrence of oceanic and continental convective systems was mostly observed between June and the first half of July. The frequency of MCS occurrence was almost null during the second half of July and in August for all years, although convective systems could be observed in some years (2007, 2008, 2010) during these months. Continental MCSs occurred practically during the monsoon period, with a higher frequency of occurrence in June and the first half of July. Oceanic MCSs also occurred between 1st June and mid-July, although in 2007, 2010, and 2013, a few convective systems occurred in September.

#### 3.4. Overview of Atmospheric Circulation and Oceanic Conditions

The study of the specific atmospheric circulation and ocean surface conditions that can help to elucidate the role of MCSs in the occurrence of extreme rainfall events is now addressed in this section. The composite patterns of these variables are displayed two days before the extreme events to take into account the atmospheric and oceanic conditions during the initiation and spreading of convective systems up to the onset date of the event. This is because MCSs can be initiated before the date of the extreme event, as noted in the previous sub-sections, and then cross the Abidjan district. The monthly composite patterns allow the highlighting of the differences in ocean surface and atmospheric conditions in each month. Note that June is the core of the rainy season, and July, August, and September correspond to the short dry season, associated with coastal and equatorial upwellings at the north of the Gulf of Guinea, and the northward migration of ITCZ. Figures 10–13 show the composite patterns of the daily SST and moisture flux anomalies at 850 hPa (left), 925 hPa (middle), and 1000 hPa (right), two days (Day-2, top) and one day (Day-1, middle) before the onset date of the extreme rainfall event, and the onset day (Day-0, bottom). The moisture flux anomaly (represented by vectors) is superimposed on each graph.

In June (Figure 10), the composite SST patterns show warming in the whole tropical Atlantic Ocean on all three days, except in the cold tongue area where a cooling is observed at the equator, in the 15° W–10° E longitudinal band. This cooling reached approximately  $-0.75$  °C and shows the onset of the equatorial upwelling located within 15° W–2.5° E at Day-2. This upwelling intensified and extended eastwards at 10° E on Day-0. Warming patterns were observed over the Brazilian Nordeste at 40° W–25° W; 5° S–6° N, along the northern coast of the Gulf of Guinea within 10° W–5° E; 3° N–5° N, and south of 3° S. In these latter three SST patterns, anomalies mostly ranged between 0.5 °C and 0.75 °C, and in some places above 0.75 °C. Beyond these patterns, SST anomalies ranged from 0.25 °C to 0.5 °C in the whole southern tropical Atlantic basin.

Oceanic warming was associated with a penetration of the moisture flow over the Abidjan district. At 850 hPa, an eastward flow of oceanic moisture was observed within 3° N–6° N; 40° W–25° W. The latitudinal location of this flow coincides with the ITCZ cloud belt in June [26,37,38]. The oceanic moisture flow at 850 hPa seemed to begin above the positive anomaly pattern close to the Nordeste from Day-2 onwards and last until Day-1. At Day-0, the moisture vectors moved slightly away, eastwards from this pattern. Therefore, it appears that this oceanic zone could provide moisture to the atmosphere, which is carried eastwards to the Abidjan district. Another area of continental moisture from the east was also observed below 9° N. The combination of these two moisture flows would supply moisture to the atmosphere, and thus help to trigger and sustain convective systems up to the day of the extreme event. The moisture flow at 925 hPa was like that at 850 hPa, but with a less pronounced pattern within the ITCZ latitudinal belt. The moisture flow at 1000 hPa was also marked by northeasterly vectors in the Gulf of Guinea, particularly off Abidjan at Day-0. These vectors cross the two positive SST anomaly patterns already

observed. This could indicate that the ocean along the northern coast of the Gulf of Guinea is also involved in moistening the atmosphere, and in supplying and sustaining the MCSs in June.

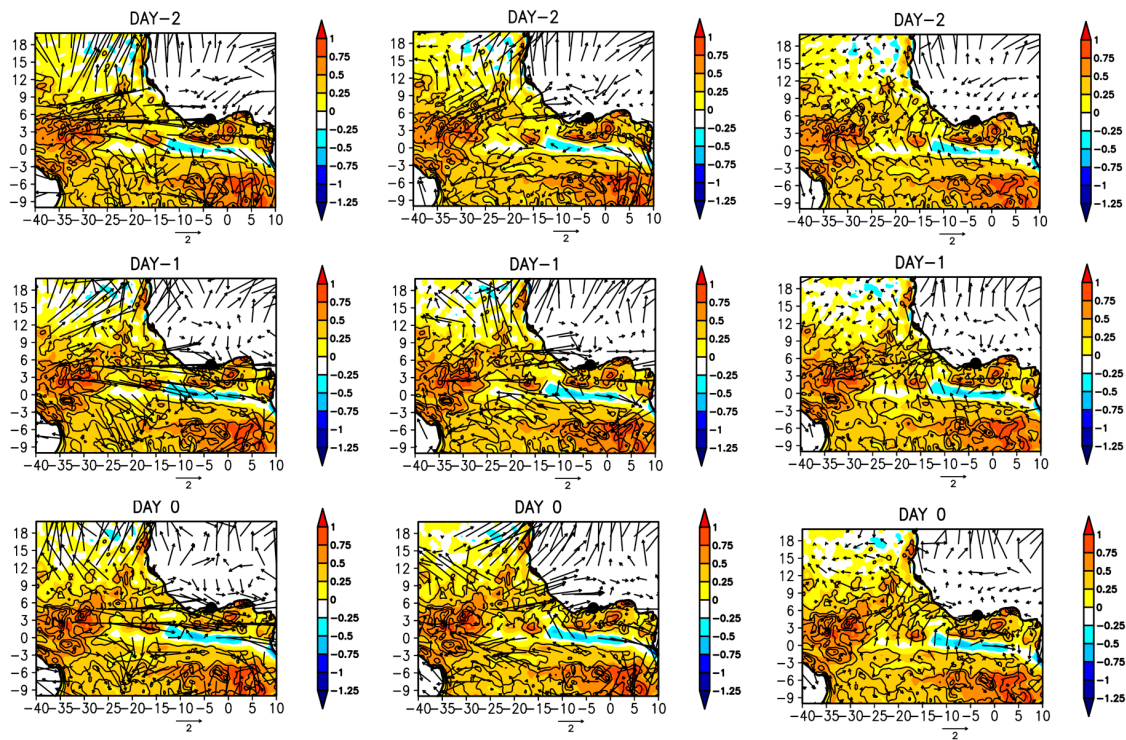


**Figure 10.** Composite patterns of daily SST anomalies (shaded) and moisture flux anomalies (arrows) at 850 hPa (left), 925 hPa (middle), and 1000 hPa (right), two days (Day-2, top) and one day (Day-1, middle) before, and on the day (Day-0, bottom) of the extreme event. Black contours provide the 95% confidence interval derived from the Student's *t*-test.

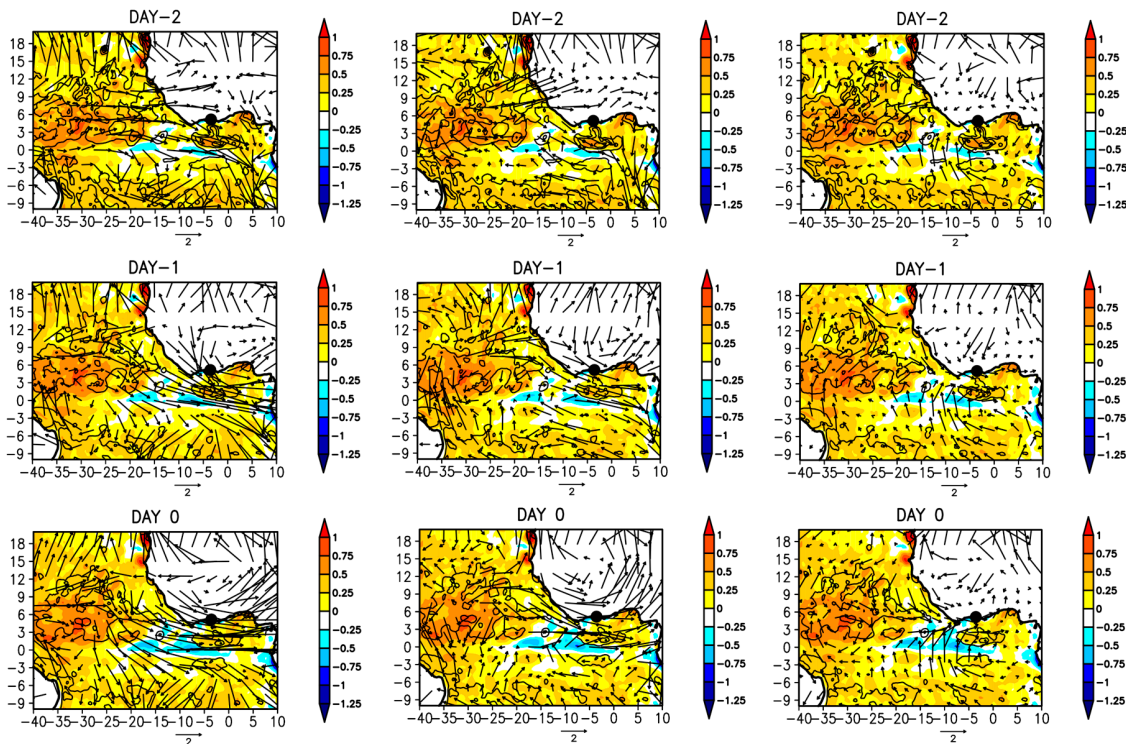


**Figure 11.** Same as Figure 10, but for July.

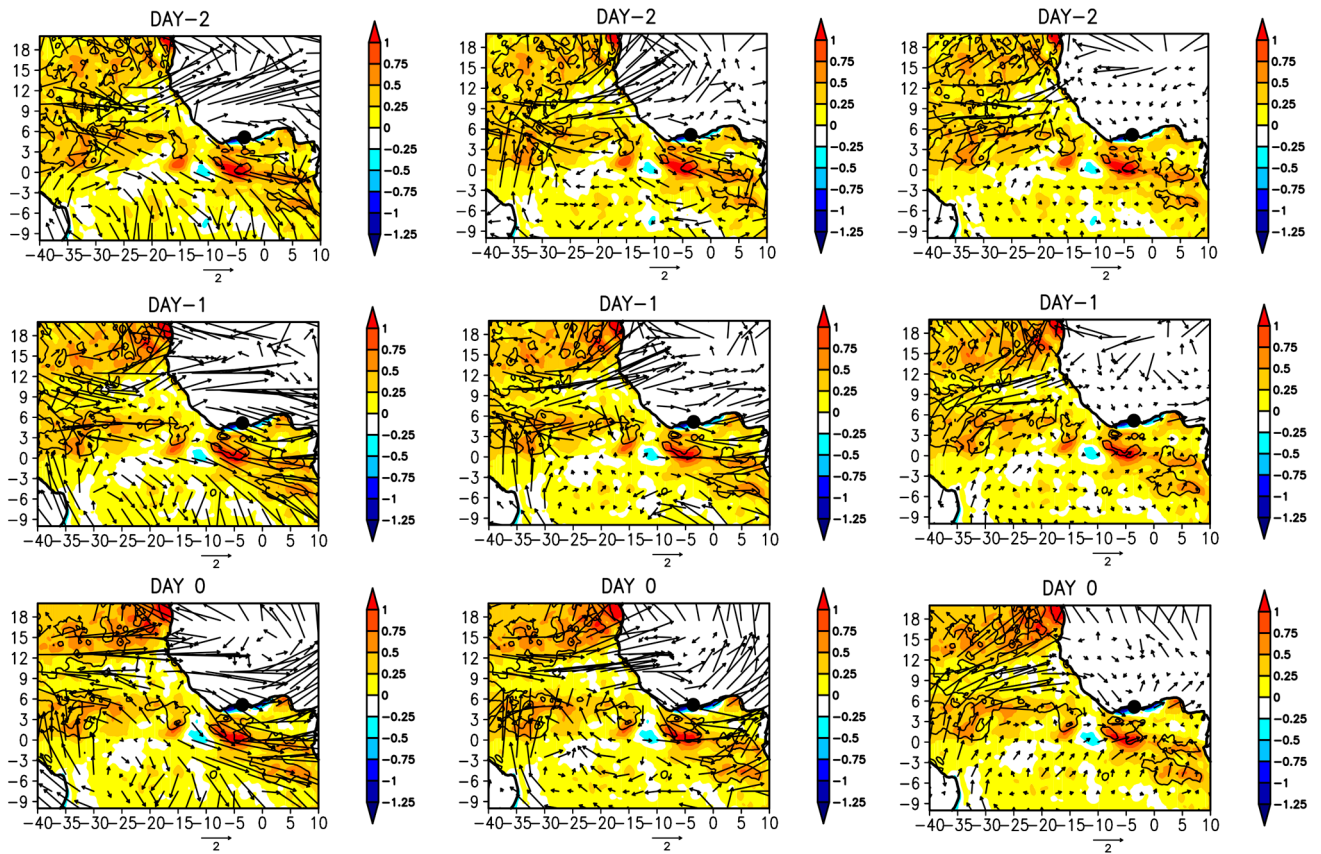


Figure 12. Same as Figure 10, but for August.

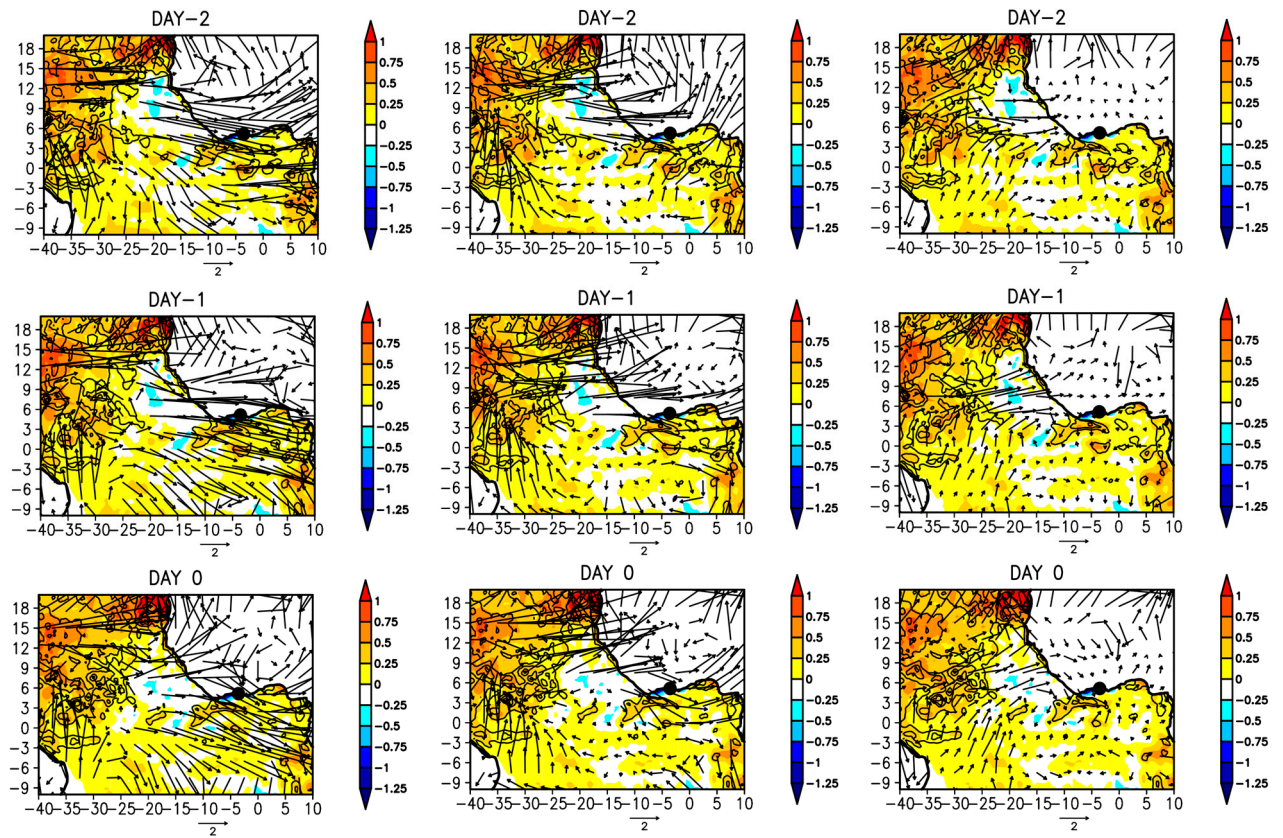


Figure 13. Same as Figure 10, but for September.

In July (Figure 11), the positive anomaly patterns of SST observed in June almost vanished, except over the Nordeste where they remained greater than  $0.75\text{ }^{\circ}\text{C}$  for the three days. The remaining northern basin had SST anomalies above  $0.5\text{ }^{\circ}\text{C}$ , while they were around  $0.25\text{ }^{\circ}\text{C}$  throughout the southern Atlantic basin. This would indicate the beginning of a cooling in the southern basin due to heat loss, and a warming of the northern basin. This discrepancy between the anomalies in the northern and the southern tropical Atlantic suggests the presence of a dipole [38,42]. This period also coincides with the upwelling in the Gulf of Guinea. Indeed, the negative SST pattern observed at the Equator in June expanded and extended to almost the whole northern coast of the Gulf of Guinea. The decrease of July anomalies compared to June would indicate an enhanced cooling of the ocean and a subsequent release of moisture fluxes that would contribute to moisten the atmosphere. This ongoing moistening could have an impact on the initiation and sustainability of convective systems.

Anomaly vectors of moisture flow at 850 hPa point out a flow from the ocean, located between  $6^{\circ}\text{ E}$  and  $10^{\circ}\text{ E}$ , moving eastwards, towards Abidjan at Day-2. This flow covered virtually the entire latitudinal band  $40^{\circ}\text{ W}$ – $0^{\circ}\text{ E}$ . In particular, this flow penetrated further into the continent towards the Abidjan district. These vectors seemed to shave the coast on the other two days. On Day-1 and Day-0, a quasi-cyclonic circulation of continental moisture flow from the east over the Abidjan district was observed over the continent, reaching this area.

At 925 hPa, the moisture flow lay in the same latitudinal band as at 850 hPa and showed similar patterns throughout the three days. However, the vectors begin around  $25^{\circ}\text{ W}$ , as opposed to 850 hPa. The longitudinal band covered by the moisture vectors towards the Abidjan district corresponds to the seasonal migration of the ITCZ during this period. At 1000 hPa, the oceanic moisture flow exhibited two components between Day-2 and Day-0. One component lay between  $6^{\circ}\text{ E}$  and  $10^{\circ}\text{ E}$ , i.e., in the northern basin of the Atlantic, and another one in the southern basin, from  $6^{\circ}\text{ S}$  to the northern coast of the Gulf of Guinea. This oceanic flow mixed with a continental flux from  $12^{\circ}\text{ N}$  for the three days.

In August (Figure 12), the core of the upwelling season in the Gulf of Guinea, the Northern Atlantic basin warmed completely. Temperature anomalies, which were about  $0.5\text{ }^{\circ}\text{C}$  at Day-2, increased to above  $0.75\text{ }^{\circ}\text{C}$  at Day-0. The anomalous warming in the northern Atlantic fell within  $0^{\circ}\text{ N}$ – $6^{\circ}\text{ N}$  and  $12^{\circ}\text{ N}$ – $20^{\circ}\text{ N}$  latitudinal bands. In the southern basin, the anomalies ranged from  $0\text{ }^{\circ}\text{C}$  to  $0.25\text{ }^{\circ}\text{C}$  on average at  $40^{\circ}\text{ W}$ – $10^{\circ}\text{ W}$ ;  $10^{\circ}\text{ S}$ – $0^{\circ}\text{ N}$ . This difference suggests the establishment of the Atlantic dipole. Abnormally warm SST patterns ( $>0.75\text{ }^{\circ}\text{C}$ ) occur along the  $2^{\circ}\text{ S}$ – $2^{\circ}\text{ N}$  equatorial rail [42–44] between  $10^{\circ}\text{ W}$  and  $5^{\circ}\text{ W}$ , and off the coast of Angola where they exceed  $0.25\text{ }^{\circ}\text{C}$ . Kouadio et al. [5] showed that abnormal warming of the ocean could occur in the Gulf of Guinea during the month of August in particular years. Such anomalous warming can influence rainfall along the northern coast of the Gulf of Guinea. Although there was abnormal warming, there were coastal ( $<-0.25\text{ }^{\circ}\text{C}$ ) and equatorial upwellings off the northern coast of the Gulf of Guinea, and in the equatorial rail between  $15^{\circ}\text{ W}$  and  $10^{\circ}\text{ W}$ .

At 850 hPa, the moisture anomaly vectors lay between  $9^{\circ}\text{ N}$  and  $15^{\circ}\text{ N}$  throughout the three days and extended mainly towards the Sahel. A similar situation was observed at 925 hPa on Day-2 and Day-1. At Day-0, the ocean moisture flow around  $6^{\circ}\text{ N}$ , from  $20^{\circ}\text{ W}$  to  $10^{\circ}\text{ W}$  crossed the continent and reached Abidjan by moving anticyclonically. Atmospheric dynamics at 1000 hPa were more distinct. There was an oceanic moisture flow along  $3^{\circ}\text{ N}$ – $15^{\circ}\text{ N}$  that was directed towards West Africa during the three days. Specifically, a part of this flow (between  $3^{\circ}\text{ N}$  and  $9^{\circ}\text{ N}$ ) rotated anticyclonically, as at 925 hPa, when penetrating the continent and reaching the Abidjan district. Nevertheless, the flow reaching Abidjan was weak when considering the size of the vectors. This could explain, firstly, the few extreme rains and the lower rainfall amounts, and secondly, the lower number of MCSs observed over Abidjan in August as compared with the previous two months.

Figure 13 displays the ocean surface conditions and atmospheric moisture flow for September. The coastal upwelling North of the Gulf of Guinea is evident, and some small

cooling patterns are apparent in the southern basin. The anomalous warming observed in August strengthened in the North Atlantic basin. The SST anomalies were almost greater than 0.75 °C in the patterns previously noted. In the southern basin, the anomalous warming in the equatorial band and off Angola had disappeared. The cooling spread throughout the southern basin, where the SST anomalies were almost lower than 0.25 °C.

The oceanic moisture anomaly at 850 hPa and 925 hPa had two components. One component in the latitudinal band 9° N–15° N corresponded to the seasonal migration of the ITCZ in this period and pointed to the Sahel during the three days. Another component, within 2° W–10° W; 3° N–9° N, moved inland to Abidjan, with strong moisture throughout the three days, notably at 850 hPa. At 1000 hPa, only the moisture flow across the 3° N–9° N band reached the Abidjan district. This flow could moisten the atmosphere and influence MCS initiation. This is consistent with previous analyses which showed that for certain years (e.g., 2007, 2010 and 2013), a few oceanic convective systems occur in September. These remarks would also explain the small number of MCSs and extreme events, and the weak rainfall during this month.

#### 4. Conclusions

This study aims to investigate the influence of convective systems on extreme rainfall along the northern coast of the Gulf of Guinea. It also diagnoses the atmospheric and oceanic influences. MCS data series from TOOCAN, and daily gridded data from the Global Precipitation Climatology Project (GPCP), National Oceanic and Atmospheric Administration (NOAA) Optimum Interpolation Sea Surface Temperature (OISST) anomalies, and moisture flux calculated from horizontal wind and specific humidity of NCEP–NCAR were used from June to September 2007–2016.

The study was carried out using statistical methods (composite and percentile) and is a valuable contribution to understanding the factors that influence extreme events in West Africa. Previous studies in this area do not connect MCSs, extreme events, and ocean–atmosphere interaction. We have linked MCSs, extreme rainfall events, and atmospheric dynamics, while quantifying the moisture input from the ocean two days before the extreme rainfall event to feed thunderstorm systems during the JJAS season. This period, which corresponds to monsoon season, includes the peak of coastal rainy season and the period of the major upwelling season off the northern coast of the Gulf of Guinea.

The results indicate that about 2/3 (~64.78%) of the MCSs that cross the Abidjan district are generated in June, which represents the heart of the rainy season. Their number drops in August (4.30%). Similarly, about 2/3 of the MCSs (~66.52%) that cross the district are continental while 1/3 (~33.68%) are oceanic. The number of oceanic convective systems decreases from June to September. This would indicate that the ocean's contribution to coastal rainfall, regarding convective systems, declines gradually with the end of the monsoon season. Oceanic MCSs are initiated mainly close to the coast within 5° W–1° E; 3.5° N–5° N, which is also the location of marine heatwaves that influence the climate of the coastal countries in West Africa. Most of the continental MCSs are initiated inland in Côte d'Ivoire and Ghana. Daily convective activity of convective systems shows that most oceanic MCSs are initiated between 00h UT and 10h UT, and dissipate between 14h and 20h UT, with lifecycles between 03h and 39.5h. Continental MCSs are initiated between 10h and 16h UT and dissipate between 16h and 00h UT, with lifecycles between 02h and 39.5h. This period of continental system initiation coincides with the maximum convection over the continent, which supplies moisture fluxes to MCSs throughout their lifecycle. The relationship between MCSs and extreme daily rainfall indicates a similar evolution of the two parameters. A large (small) number of MCSs is generally associated with a heavy (weak) rainy year.

Finally, the study of specific atmospheric circulation and ocean surface conditions that can help to understand MCS influence on the occurrence of extreme rainfall events is also addressed. It was carried out monthly to highlight the differences in ocean surface and atmospheric conditions occurring each month. The results illustrate the contribution

of moisture flux from three zones to the initiation and sustain of the MCSs that influence the extreme events studied: (i) the oceanic moisture flux from the seasonal migration band of the ITCZ during JJAS, (ii) the oceanic moisture flux in the Gulf of Guinea across the northern coastline where coastal upwelling and marine heatwaves occur in the southern Atlantic basin, and (iii) the continental moisture flux. The moisture inflow in the ITCZ oceanic band coincides with a significant oceanic warming over the Nordeste ( $>0.75$  °C) two days before and the day of the extreme rainfall event. In the case of the northern coast of the Gulf of Guinea ( $10^{\circ}$  W– $5^{\circ}$  E;  $3^{\circ}$  N– $5^{\circ}$  N), the anomalies range from  $0.5$  °C to  $0.75$  °C. These observations indicate that the ocean, through these two zones, contributes by moistening the atmosphere, and therefore by supplying and sustaining the MCSs. An important remark is the weak flow amount that reaches Abidjan in August. This would explain the small number of MCSs and extreme events, and the weak rainfall.

This study indicates that ocean–atmosphere processes can be used to improve the forecasting of MCS dynamics and extreme rainfall episodes over West Africa and could increase our warning capacity for severe weather conditions in that region. Initiatives of coupled model simulations could then give one a useful dynamical basis for such ocean–atmosphere processes. It could be useful to better explain the extreme rainfall phenomena. It could also help in planning the risks associated with these climate hazards, particularly in water resource management and civil defense.

**Author Contributions:** Writing—original draft preparation, reviewing, S.D.; data curation, formal analysis, methodology, reviewing, J.A.; formal analysis, writing—original draft preparation, supervision, conceptualization, K.Y.K.; software, reviewing, M.K. All authors have read and agreed to the published version of the manuscript.

**Funding:** This research received no external funding.

**Institutional Review Board Statement:** Not applicable.

**Informed Consent Statement:** Not applicable.

**Data Availability Statement:** MCS data are provided by Fiolleau and Roca (see Acknowledgements). All reanalysis data used in this study are publicly available. Please refer to Section 2 for the sources.

**Acknowledgments:** We kindly acknowledge Remy Roca (remy.roca@legos.obs-mip.fr) and Thomas Fiolleau (thomas.fiolleau@legos.obs-mip.fr), both researchers at LEGOS, a laboratory of the Observatoire Midi-Pyrénées in Toulouse, for making the TOOCAN database used for this research work freely available. We are grateful to the anonymous reviewers for their helpful comments and suggestions, which helped improve the quality of this paper.

**Conflicts of Interest:** The authors declare no conflict of interest.

## Appendix A

The surfaces of the district of Abidjan ( $\sim 2119$  km<sup>2</sup>) and the MCSs were assumed to be circular to facilitate the study. We have noted  $r \sim 2119$  km as the radius of the city of Abidjan, and the  $R_{cluster}$  of the MCS at time  $t$ . The 15 min spreading areas of MCSs are represented here as circles proportional to the cloud-covered area according to the method of Kouadio et al. [45].

The coordinates of the center of Abidjan are taken as  $x_a = 4.013^{\circ}$  W for longitude and  $y_a = 5.3^{\circ}$  N for latitude. In the case of MCSs, the coordinates of the center of mass ( $x_b$  and  $y_b$ ) are used. They vary in time depending on the trajectory of the system. The distance between the centre of mass of the system at time  $t$  and Abidjan (Figure A1a) is given by:

$$D_i(t) = \sqrt{(x_b - x_a)^2 + (y_b - y_a)^2} = R_{cluster} + X + r$$

The aim is to minimize the absolute value of the distance  $X = D_i(t) - (R_{cluster} + r)$ , so that the system covers Abidjan entirely or partially.

If  $X = 0$ , i.e.,  $\llbracket D_i(t) = (R_{cluster} + r) \rrbracket$ , then the system razes the city of Abidjan without penetrating (Figure A1b). This case is not relevant to the study.

However, if  $X < 0$ , i.e.,  $\llbracket D_i(t) < (R_{cluster} + r)$ , then the system enters the city of Abidjan (Figure A1c). This case is interesting for the study. To increase the probability that rain occurs in the city due to the system, we consider that the absolute value of  $X$  is at least equal to 1/3 of the radius of the city of Abidjan, i.e., approximately 8.66 km (Figure A1b). This means that the system has sufficiently reached the city of Abidjan to have an impact.

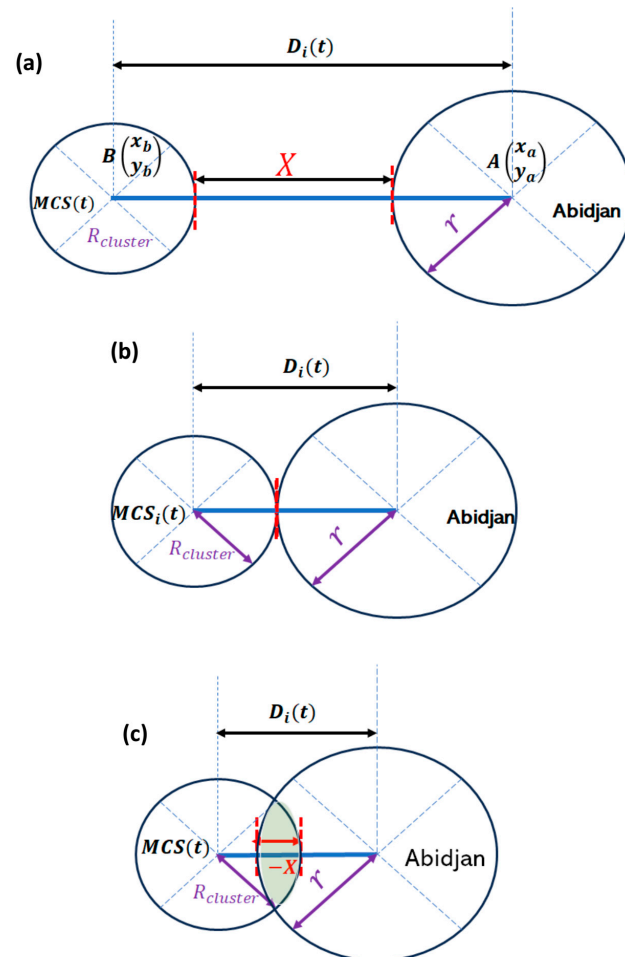


**Figure A1.** Schematic diagram of the selection of MCSs that cross Abidjan. (a) The general case, (b) rejected case, and (c) selected case. The absolute value of  $X$  represents the distance to be minimized in the case of selected MCSs. The grey area represents the surface covered by the MCS.

## References

1. Tomasini, M.; Lafore, J.P.; Piriou, C.; Roca, R.; Ramage, K.; Laurent, H.; Morel, C.; Senesi, S. Atlas on a Climatology of West African Mesoscale Convective Systems. *AMMA Eur. Deliv.* **2006**. Available online: [https://d1wqtxts1xzle7.cloudfront.net/50451864/ATLAS\\_on\\_a\\_climatology\\_of\\_West\\_African\\_M20161121-9766-12iy4n9-libre.pdf?1479722653\protect\unhbox\voidb@x\hbox{=&response-content-disposition=inline%3B+filename%3DATLAS\\_on\\_a\\_climatology\\_of\\_West\\_African\\_M.pdf&Expires=1698051746&Signature=cixcy~V3cNbvBOUMoII~Zb4jbxdfJh5IqRpbf0JdesnkxjbjKimTFvRsyJNC~J76ZDcAOLG8fXlrwLmet3f0p9B6KzNffin7AIJAPaYSFZ94MYhzeebkdJTHf3nxxh~CJV4cr-vplaECFViKINscPWEEcwj1IBU~TESurh5dmJpHB{-}{-}Ilg2DtTesuOya-b0Wa-qxVt-qjSkVVmAt259tKOpSDlFVdaPZn4e3e47kjd~Qg1kz5RKmmVaYpYxHr8GiVsE6bedW3W9JJyKgBPKUpdNbNtzxL9EtbFuFhWFClYMXju1InyGX~JRIHqfOQk0eVrbOBP60wY-U~cV62y5qhBg\\_&Key-Pair-Id=APKAJLOHF5GGSLRBV4ZA](https://d1wqtxts1xzle7.cloudfront.net/50451864/ATLAS_on_a_climatology_of_West_African_M20161121-9766-12iy4n9-libre.pdf?1479722653\protect\unhbox\voidb@x\hbox{=&response-content-disposition=inline%3B+filename%3DATLAS_on_a_climatology_of_West_African_M.pdf&Expires=1698051746&Signature=cixcy~V3cNbvBOUMoII~Zb4jbxdfJh5IqRpbf0JdesnkxjbjKimTFvRsyJNC~J76ZDcAOLG8fXlrwLmet3f0p9B6KzNffin7AIJAPaYSFZ94MYhzeebkdJTHf3nxxh~CJV4cr-vplaECFViKINscPWEEcwj1IBU~TESurh5dmJpHB{-}{-}Ilg2DtTesuOya-b0Wa-qxVt-qjSkVVmAt259tKOpSDlFVdaPZn4e3e47kjd~Qg1kz5RKmmVaYpYxHr8GiVsE6bedW3W9JJyKgBPKUpdNbNtzxL9EtbFuFhWFClYMXju1InyGX~JRIHqfOQk0eVrbOBP60wY-U~cV62y5qhBg_&Key-Pair-Id=APKAJLOHF5GGSLRBV4ZA) (accessed on 26 August 2023).
2. Mathon, V.; Laurent, H.; Lebel, T. Mesoscale Convective System Rainfall in the Sahel. *J. Appl. Meteor.* **2002**, *41*, 1081–1092. [[CrossRef](#)]
3. Ta, S.; Kouadio, K.Y.; Ali, K.E.; Toualy, E.; Aman, A.; Yoroba, F. West Africa Extreme Rainfall Events and Large-Scale Ocean Surface and Atmospheric Conditions in the Tropical Atlantic. *Adv. Meteorol.* **2016**, *2016*, 1940456. [[CrossRef](#)]
4. Lafore, J.-P.; Beucher, F.; Peyrillé, P.; Diongue-Niang, A.; Chapelon, N.; Bouniol, D.; Caniaux, G.; Favot, F.; Ferry, F.; Guichard, F.; et al. A Multi-Scale Analysis of the Extreme Rain Event of Ouagadougou in 2009: Extreme Rain Event in Burkina Faso. *Q. J. R. Meteorol. Soc.* **2017**, *143*, 3094–3109. [[CrossRef](#)]

5. Kouadio, Y.K.; Ochou, D.A.; Servain, J. Tropical Atlantic and Rainfall Variability in Côte d'Ivoire. *Geophys. Res. Lett.* **2003**, *30*, 8005. [[CrossRef](#)]
6. Kouadio, K.Y.; Aman, A.; Ochou, A.D.; Ali, K.E.; Assamoi, P.A. Rainfall Variability Patterns in West Africa: Case of Cote d'Ivoire and Ghana. *J. Environ. Sci. Eng.* **2011**, *5*, 1229–1238.
7. Damania, R.; Desbureaux, S.; Zaveri, E. Does Rainfall Matter for Economic Growth? Evidence from Global Sub-National Data (1990–2014). *J. Environ. Econ. Manag.* **2020**, *102*, 102335. [[CrossRef](#)]
8. Santé, N.; N'Go, Y.; Soro, G.E.; Meledje, N.D.H.; Goula, B.T.A. Characterization of Meteorological Droughts Occurrences in Côte d'Ivoire: Case of the Sassandra Watershed. *Climate* **2019**, *7*, 60. [[CrossRef](#)]
9. Konate, D.; Didi, S.R.; Dje, K.B.; Diedhiou, A.; Kouassi, K.L.; Kamagate, B.; Patuere, J.-E.; Coulibaly, H.S.J.-P.; Kouadio, C.A.K.; Coulibaly, T.J.H. Observed Changes in Rainfall and Characteristics of Extreme Events in Côte d'Ivoire (West Africa). *Hydrology* **2023**, *10*, 104. [[CrossRef](#)]
10. Ochou, A.D.; Aman, A.; Kouadio, K.Y.; Assamoi, P. Nouveau Zonage Climatique Basé Sur La Variabilité Pluviométrique En Côte d'Ivoire et Au Ghana. *Geotrope* **2005**, *5*, 34–46.
11. Amouin, J.; Kouadio, K.Y.; Kacou, M.; Djakouré, S.; Ta, S. Diagnosis of the Causes of the Rain Flooding in June in the West Africa Coastal Area. *ACS* **2021**, *11*, 11–31. [[CrossRef](#)]
12. OCHA. Côte d'Ivoire: Zones à Risques d'inondations et de Choléra—Portail Sur La Résilience Aux Inondations. Available online: <https://resilience-inondations.net/ressources/item/cote-divoire-zones-a-risques-dinondations-et-de-cholera/> (accessed on 28 July 2023).
13. UN-HABITAT. Profil Urbain de La Ville d'Abidjan, Édité Par Le Programme Des Nations Unies Pour Les Établissements Humains—Recherche Google. Available online: <https://unhabitat.org/sites/default/files/download-manager-files/Cote%20d%20Ivoire%20-%20Abidjan.pdf> (accessed on 26 August 2023).
14. Reason, C.J.C.; Rouault, M. Sea Surface Temperature Variability in the Tropical Southeast Atlantic Ocean and West African Rainfall. *Geophys. Res. Lett.* **2006**, *33*, L21705. [[CrossRef](#)]
15. Lutz, K.; Jacobeit, J.; Rathmann, J. Atlantic Warm and Cold Water Events and Impact on African West Coast Precipitation: Atlantic SST and African West Coast Precipitation. *Int. J. Climatol.* **2015**, *35*, 128–141. [[CrossRef](#)]
16. Panthou, G.; Vischel, T.; Lebel, T.; Blanchet, J.; Quantin, G.; Ali, A. Extreme Rainfall in West Africa: A Regional Modeling: Extreme Rainfall Mapping West Africa. *Water Resour. Res.* **2012**, *48*, W08501. [[CrossRef](#)]
17. Ibrahim, B.; Polcher, J.; Karambiri, H.; Rockel, B. Characterization of the Rainy Season in Burkina Faso and It's Representation by Regional Climate Models. *Clim. Dyn.* **2012**, *39*, 1287–1302. [[CrossRef](#)]
18. Goula, B.T.A.; Soro, E.G.; Kouassi, W.; Srohourou, B. Tendances et Ruptures Au Niveau Des Pluies Journalières Extrêmes En Côte d'Ivoire (Afrique de l'Ouest). *Hydrol. Sci. J.* **2012**, *57*, 1067–1080. [[CrossRef](#)]
19. Machado, L.A.T.; Rossow, W.B. Structural Characteristics and Radiative Properties of Tropical Cloud Clusters. *Mon. Wea. Rev.* **1993**, *121*, 3234–3260. [[CrossRef](#)]
20. Machado, L.A.T.; Guedes, R.L.; Alves, M.A.S. Structural Characteristics of Convective Systems and Forcing of Convection in South America Observed by Satellites (Características Estruturais de Sistemas Convectivos e Forçantes da Convecção Na América Do Sul Observados Por Satélites). *Edição Comemorativa Anos Climanálise* **1997**, 110–122.
21. Machado, L.A.T.; Laurent, H. The Convective System Area Expansion over Amazonia and Its Relationships with Convective System Life Duration and High-Level Wind Divergence. *Mon. Wea. Rev.* **2004**, *132*, 714–725. [[CrossRef](#)]
22. Mathon, V.; Diedhiou, A.; Laurent, H. Relationship between Easterly Waves and Mesoscale Convective Systems over the Sahel: Relationship between Easterly Waves and Mesoscale Convective Systems Over The Sahel. *Geophys. Res. Lett.* **2002**, *29*, 57-1–57-4. [[CrossRef](#)]
23. Fiolleau, T.; Roca, R. Composite Life Cycle of Tropical Mesoscale Convective Systems from Geostationary and Low Earth Orbit Satellite Observations: Method and Sampling Considerations: Composite Life Cycle of Tropical Mesoscale Convective Systems. *Q. J. R. Meteorol. Soc.* **2013**, *139*, 941–953. [[CrossRef](#)]
24. Maranan, M.; Fink, A.H.; Knippertz, P.; Francis, S.D.; Akpo, A.B.; Jegede, G.; Yorke, C. Interactions between Convection and a Moist Vortex Associated with an Extreme Rainfall Event over Southern West Africa. *Mon. Weather. Rev.* **2019**, *147*, 2309–2328. [[CrossRef](#)]
25. Atiah, W.A.; Amekudzi, L.K.; Danuor, S.K. Mesoscale Convective Systems and Contributions to Flood Cases in Southern West Africa (SWA): A Systematic Review. *Weather Clim. Extrem.* **2023**, *39*, 100551. [[CrossRef](#)]
26. Sultan, B.; Janicot, S.; Drobinski, P. Characterization of the Diurnal Cycle of the West African Monsoon around the Monsoon Onset. *J. Clim.* **2007**, *20*, 4014–4032. [[CrossRef](#)]
27. Huffman, G.J.; Adler, R.F.; Morrissey, M.M.; Bolvin, D.T.; Curtis, S.; Joyce, R.; McGavock, B.; Susskind, J. Global Precipitation at One-Degree Daily Resolution from Multisatellite Observations. *J. Hydrometeor.* **2001**, *2*, 36–50. [[CrossRef](#)]
28. Laurent, H. Characteristics of the Amazonian Mesoscale Convective Systems Observed from Satellite and Radar during the WETAMC/LBA Experiment. *J. Geophys. Res.* **2002**, *107*, 8054. [[CrossRef](#)]
29. Reynolds, R.W.; Rayner, N.A.; Smith, T.M.; Stokes, D.C.; Wang, W. An Improved In Situ and Satellite SST Analysis for Climate. *J. Clim.* **2002**, *15*, 1609–1625. [[CrossRef](#)]
30. Kalnay, E.; Kanamitsu, M.; Kistler, R.; Collins, W.; Deaven, D.; Gandin, L.; Iredell, M.; Saha, S.; White, G.; Woollen, J.; et al. The NCEP/NCAR 40-Year Reanalysis Project. *Bull. Amer. Meteor. Soc.* **1996**, *77*, 437–471. [[CrossRef](#)]

31. Frei, C.; Schär, C. Detection Probability of Trends in Rare Events: Theory and Application to Heavy Precipitation in the Alpine Region. *J. Clim.* **2001**, *14*, 1568–1584. [[CrossRef](#)]
32. Klein Tank, A.M.G.; Können, G.P. Trends in Indices of Daily Temperature and Precipitation Extremes in Europe, 1946–1999. *J. Clim.* **2003**, *16*, 3665–3680. [[CrossRef](#)]
33. Haylock, M.R.; Peterson, T.C.; Alves, L.M.; Ambrizzi, T.; Anunciação, Y.M.T.; Baez, J.; Barros, V.R.; Berlato, M.A.; Bidegain, M.; Coronel, G.; et al. Trends in Total and Extreme South American Rainfall in 1960–2000 and Links with Sea Surface Temperature. *J. Clim.* **2006**, *19*, 1490–1512. [[CrossRef](#)]
34. Zakaria, R.; Ahmad Radi, N.F.; Satari, S.Z. Extraction Method of Extreme Rainfall Data. *J. Phys. Conf. Ser.* **2017**, *890*, 012154. [[CrossRef](#)]
35. Demirdjian, L.; Zhou, Y.; Huffman, G.J. Statistical Modeling of Extreme Precipitation with TRMM Data. *J. Appl. Meteorol. Climatol.* **2018**, *57*, 15–30. [[CrossRef](#)]
36. Brown, T.J.; Hall, B.L. The Use of t Values in Climatological Composite Analyses. *J. Clim.* **1999**, *12*, 2941–2944. [[CrossRef](#)]
37. Roldán-Gómez, P.J.; González-Rouco, J.F.; Melo-Aguilar, C.; Smerdon, J.E. The Role of Internal Variability in ITCZ Changes Over the Last Millennium. *Geophys. Res. Lett.* **2022**, *49*, e2021GL096487. [[CrossRef](#)]
38. Xie, S.-P. Tropical Atlantic Variability. In *Coupled Atmosphere-Ocean Dynamics*; Elsevier: Amsterdam, The Netherlands, 2023; pp. 251–276, ISBN 978-0-323-95490-7.
39. Djakouré, S.; Penven, P.; Bourlès, B.; Koné, V.; Veitch, J. Respective Roles of the Guinea Current and Local Winds on the Coastal Upwelling in the Northern Gulf of Guinea. *J. Phys. Oceanogr.* **2017**, *47*, 1367–1387. [[CrossRef](#)]
40. Koné, M.; Djakouré, S.; Adon, M.; Ta, S.; Kouadio, Y. Marine Heatwaves, Upwelling, and Atmospheric Conditions during the Monsoon Period at the Northern Coast of the Gulf of Guinea. *Climate* **2022**, *10*, 199. [[CrossRef](#)]
41. Rasera, G.; Anabor, V.; Scremin Puhales, F.; Dal Piva, E. Developing an MCS Index Using the Climatology of South America: South American Mesoscale Convective System Index. *Met. Apps* **2018**, *25*, 394–405. [[CrossRef](#)]
42. Servain, J.; Wainer, I.; Ludos Ayina, H.; Roquet, H. The Relationship between the Simulated Climatic Variability Modes of the Tropical Atlantic. *Int. J. Climatol.* **2000**, *20*, 939–953. [[CrossRef](#)]
43. Servain, J. Réponse Océanique à Des Actions Éloignées Du Vent Dans Le Golfe de Guinée En 1967–1968. *Oceanol. Acta* **1984**, *7*, 297–307.
44. Servain, J. Simple Climatic Indices for the Tropical Atlantic Ocean and Some Applications. *J. Geophys. Res.* **1991**, *96*, 15137. [[CrossRef](#)]
45. Kouadio, Y.K.; Servain, J.; Machado, L.A.; Lentini, C.A. Heavy Rainfall Episodes in the Eastern Northeast Brazil Linked to Large-Scale Ocean-Atmosphere Conditions in the Tropical Atlantic. *Adv. Meteorol.* **2012**, *2012*, 369567. [[CrossRef](#)]

**Disclaimer/Publisher’s Note:** The statements, opinions and data contained in all publications are solely those of the individual author(s) and contributor(s) and not of MDPI and/or the editor(s). MDPI and/or the editor(s) disclaim responsibility for any injury to people or property resulting from any ideas, methods, instructions or products referred to in the content.